Late-Pleistocene evolution of the continental shelf of central Israel, a case study from Hadera

Gilad Shtienberg [a,*], Justin Dix [b], Nicolas Waldmann [c], Yizhaq Makovsky [c], Arik Golan [d], Dorit Sivan [a,e]

[a] Department of Maritime Civilizations, L. H. Charney School of Marine Sciences, University of Haifa, 31905 Haifa, Israel
[b] The School of Ocean and Earth, University of Southampton, Southampton SO14 3ZH, UK
[c] Dr. Moses Strauss Department of Marine Geosciences, L. H. Charney School of Marine Sciences, University of Haifa, 31905 Haifa, Israel
[d] Israel Oceanographic and Limnological Research Institute, 31080 Haifa, Israel
[e] The Recanati Institute for Maritime Studies (RIMS), University of Haifa, 31905 Haifa, Israel

ARTICLE INFO

ABSTRACT

Sea-level fluctuations are a dominant mechanism that control coastal environmental changes through time. This is especially the case for the successive regressions and transgressions over the last interglacial cycle, which have shaped the deposition, preservation and erosion patterns of unconsolidated sediments currently submerged on continental shelves. The current study focuses on creating an integrated marine and terrestrial geophysical and litho-stratigraphic framework of the coastal zone of Hadera, north-central Israel. This research presents a case study, investigating the changing sedimentological units in the study area. Analysis suggest these represent various coastal environments and were deposited during times of lower than present sea level and during the later stages of the Holocene transgression.

A multi-disciplinary approach was applied by compiling existing elevation raster grids, bathymetric charts, one hundred lithological borehole data-sets, and a 110 km-long sub-bottom geophysical survey. Based on seismic stratigraphic analysis, observed geometries, and reflective appearances, six bounding surfaces and seven seismic units were identified and characterized. These seismic units have been correlated with the available borehole data to produce a chronologically constrained lithostratigraphy for the area. This approach allowed us to propose a relationship between the lithological units and sea-level change and thus enable the reconstruction of Hadera coastal evolution over the last ~100 ka. This reconstruction suggests that the stratigraphy is dominated by lowstand aeolian and fluvial terrestrial environments, subsequently transgressed during the Holocene. The results of this study provide a valuable framework for future national strategic shallow-water infrastructure construction and also for the possible locations of past human settlements in relation to coastal evolution through time.

© 2016 Elsevier B.V. All rights reserved.

1. Introduction

The "coastal" zone, which encompasses both current terrestrial and marine environments, frequently contains sedimentary sequences which can provide detailed records of changing depositional environments and ecosystems in response to climate change and sea-level fluctuations. Prior studies that have examined these coastal areas and their response to past sea level and climate change have largely focused on sheltered environments such as estuaries and deltas, as the preservation potential within these settings is exceptionally high (e.g. Belknap and Kraft, 1985; Allard et al., 2009; Zecchin et al., 2009). More recently researchers have started to examine the response of open coastlines to these same drivers, with particular focus on the response to the Late Pleistocene to Holocene transgression (e.g. Zecchin et al., 2008; Yoo et al., 2014; Mendoza et al., 2014). However, these latter studies have focused exclusively on the current offshore record with relatively few attempts being made to tie together the terrestrial and littoral components of the coastal zone (Bersezio et al., 2007; Stoker et al., 2009; Peterson et al., 2010; Twichell et al., 2010; Vanderburgh et al., 2010; Anderson et al., 2014; Cawthra et al., 2014). The partial mapping and dating of open coastline shallow shelf sediments and the complexities in correlating to onshore equivalents, posed difficulties to fully understand the global and local factors shaping and altering the shallow marine areas (Bates et al., 2007; Hampson and Storms, 2008).

This paper focuses on a case study, from the open coastline of central Israel and attempts to combine data from both the marine and terrestrial components of its coastal zone. The Israeli coast (Fig. 1) suits this kind of study as: it is micro-tidal (±0.40 m) (Emery and Neev, 1960; Davis and Hayes, 1984; Golik and Rosen, 1999); its continental shelf is
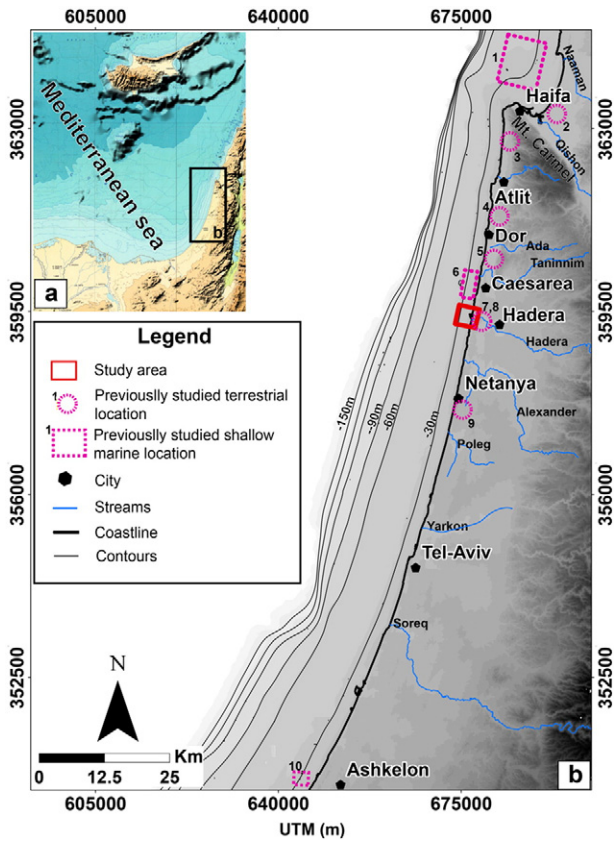
Fig. 1. Location maps of Israel in SE Mediterranean (a) and the relevant studies conducted in Israel's coastal and shallow shelf. The black square demonstrates the location of panel b; the red square represents the study area; the numbered dashed purple circle represent previously studied zones on the terrestrial side; the numbered purple dashed square represents previously studied zones in the shallow shelf area. The previously studied zones are described in the following papers according to their numbering: (1) Schattner et al. (2010); (2) Zviely et al. (2007); (3) Galili and Weinstein-Evron (1985); (4) Kadosh et al. (2004); Sivan et al. (2004a); (5) Cohen-Seffer et al. (2005); Sivan et al. (2011); (6) Neev et al. (1978); Goodman-Tchernov et al. (2009); (7) Roskin et al. (8) Frechen et al. (2001); (9) Engelmann et al. (2001); and (10) Porat et al. (2003a).

characterized by a relatively narrow (10 to 23 km) and moderately steep (0.5° to 0.8°) strip of mostly unconsolidated sediments that have been largely supplied by a single dominant source since the Pliocene (the Nile River e.g. Emery and Bentor, 1960; Neev et al., 1976; Almagor and Hall, 1984; Almagor, 1993; Stanley and Warne, 1998); it is considered tectonically stable since MIS5e (Sivan et al., 1999; Galili et al., 2007; Mauz et al., 2013), with low isostatic rates of 0.1 mm/year, at least in the Holocene (Sivan et al., 2001; Anzidei et al., 2011; Toker et al., 2012); there is currently little known about the timing and extent of the shallow shelf subsurface stratigraphy.

Inquiry of the shallow shelf stratigraphy is achieved through a combination of dense offshore sub-bottom profiles, bathymetry (from water depth of −5 to −30 m), topography data and onshore and offshore cores. The integration and analysis of these data-sets allows the generation of a time-lapse paleo-environmental reconstruction for the last ~100 ka in the area of Hadera on the central Israeli coast. In addition to providing a detailed case study of coastal change for an open coast setting, this work also provides insight into the process of change in an area that is currently undergoing rapid onshore and offshore infrastructure development. Finally, the knowledge gained from this research also benefits archaeologists in evaluating locations suited for finding ancient settlements now submerged under the sea bed.

2. Regional setting

The width of Israel's coastal plain varies from a few hundred meters, in its northern parts up to 15 km south of Mt. Carmel (Almagor and Hall, 1984). The morphology of the coast and immediate hinterland of Israel (Fig. 1b) is dominated by up to eighteen aeolianite ridges that trend, parallel-subparallel to the current 190 km-long relatively straight coastline. These ridges, which are identified both onshore and offshore (Neev et al., 1978; Almagor et al., 2000; Frechen et al., 2001, 2002, 2004a, 2004b; Sivan and Porat, 2004; Sivan et al., 2004a; Schattner et al., 2010), were formed during the late Pleistocene when sea levels were lower than present and the shelf was exposed (Mauz et al., 2013). The Nile littoral cell system (Emery and Neev, 1960; Pomerancblum, 1966; Davis et al., 2012) supplied quartz-rich sands (with minor litho- and bio-clasts) from the Nile Delta to the Levant shelf (shallower then 40 m water depth). Wave- and wind-induced currents subsequently transported these sediments landward and once on the beach, these sands were blown inland to accumulate on the coastal plain as a series of shore-parallel dunes. Through the dissolution of carbonate skeletal debris within the sand by meteoric waters and its precipitation as calcite cement, the dunes underwent lithification to create the sandstone aeolianites, known locally as Kurkar (Yaalon, 1967; Gavish and Friedman, 1969; Almagor et al., 2000; Mauz et al., 2013). The number and size of these ridges diminishes northward and only three are found onshore west of Mount Carmel (Michelson, 1970; Sneh and Rosensaft, 1998).

The trough regions between these parallel Kurkar ridges are filled with up to ~20 m thick sequences of unconsolidated sediments. These sediments include additional Nilotic derived aeolian sediments which pedogenized under different climatic conditions (Yaalon, 1997; Gvirtzman et al., 1998; Gvirtzman and Wieder, 2001) to orange silty sand and brown clayey silty sand (locally known as Hamra and Brown-Paleosol units respectively). These soils are covered by wetland dark silty clays and/or aeolian sand (Gvirtzman et al., 1998; Kadosh et al., 2004; Sivan and Porat, 2004; Sivan et al., 2004a, 2011, Zviely et al., 2006).

While the topmost surface of the Pleistocene Kurkar unit has been chronologically constrained to between ~101 and ~50 ka (Engelmann et al., 2001; Frechen et al., 2004b; Sivan and Porat, 2004; Sivan et al., 2004a; Zviely et al., 2006; Roskin et al., 2015) there is no spatial pattern to the varying ages of the Kurkar ridges and the relationships between them and former sea-level changes have still not been properly established (Sivan and Porat, 2004; Mauz et al., 2013). Most of our understanding of the Kurkar, its chronology and morphology, comes from studies carried out on exposed terrestrial outcrops, leaving the extent and ages of the offshore submerged Kurkar mostly unknown. Offshore, the Kurkar has only been sporadically mapped by seismic profiling (Neev et al., 1978; Belknap and Mart, 1999; Almagor et al., 2000; Schattner et al., 2010) and even more limited sea floor observations carried out by ROVs and side scan sonar (Mart and Belknap, 1991; Belknap and Mart, 1999).

The overlying Hamra and Brown-Paleosol units have been shown to have a wide range of ages, from ~87 to ~55 ka and ~50 to ~11 ka respectively (Frechen et al., 2001, 2004b; Gvirtzman and Wieder, 2001; Cohen-Seffer et al., 2005; Roskin et al., 2015), so are sometimes synchronous with the Kurkar's formation (Sivan and Porat, 2004) and sometimes younger. These two units contain various sub-units and hiatuses, which probably indicate long exposure to pedogenic processes, hence impeding proper lateral chronostratigraphical correlations (Sivan and Porat, 2004). In the coastal areas of north and central Israel the Hamra and Brown-Paleosol units reach a maximum thickness of 8 m. Particle size and hue values change spatially and temporally, apparently following the paleotopography (Sivan and Porat, 2004) and/or dictated by phases of wet/dry paleoclimate (Neev et al., 1978; Wieder et al., 1997; Yaalon, 1997; Gvirtzman et al., 1998).

A dark silty clay unit, rich in organic material, interpreted to originate from freshwater to brackish wetland marshes, unconformably overlies the Hamra/Brown-Paleosol sequence (Galili and Weinstein-Evron, 1985; Sivan et al., 2011). Dating of this unit onshore and in two shallow offshore core locations in southern and north-central Israel (Fig. 1), reveals that the wetlands prevailed between 14.4 and 8.4 cal. kyr BP (Neev et al., 1978; Sivan et al., 1999, 2004a; Porat et al., 2003a). The creation of these wetlands and the underlying erosional unconformity of the Hamra/Brown-Paleosol units may be related to a combination of early Holocene wet climate conditions, sand dune obstruction of fluvial outlets due to increasing sedimentation rates, as well as the indirect effects of sea-level rise on groundwater levels (Kadosh et al., 2004; Cohen-Seffer et al., 2005; Sivan et al., 2011).

Rohling et al. (2014) have produced the longest (up to 5.3 Myr) continuous Mediterranean, eustatic, sea-level record based on $\delta^{18}O$ from carbonate microfossils, whilst Lambeck and Purcell (2005) present a GIA model for the Mediterranean that extends back to the Last Glacial Maximum (LGM; c. 20 ka). All other Israeli relative sea-level curves only cover the Holocene (e.g. Sivan et al., 2001). A simplistic reconstruction based on the Rohling et al. (2014) sea level data and the modern day bathymetry of the Israeli continental shelf (used as a lowstand land surface proxy) can give an indication of the extent of shoreline migration over the last ~100 ka. From ~100 ka sea levels dropped from −30 m to a minimum of −135 m during the LGM. Accordingly the shoreline migrated seaward from 3 km at ~100 ka to ~10 km offshore at the LGM. Since the LGM, global sea levels have risen dramatically, reaching ~35 m below present MSL by the beginning of the Holocene. Archaeological observations from the coast of Israel indicate that sea levels continued to rise until ~6 ka to ~7 ka when rates of sea level rise slowed considerably and the shoreline was located ~3 km offshore from its current location. Sea level almost reached its present elevation at ~4 ka (Sivan et al., 2001, 2004b; Anzidei et al., 2011; Toker et al., 2012), and the coastline prograded to reach its present location at ~3 ka (Kadosh et al., 2004; Cohen-Seffer et al., 2005; Zviely et al., 2006, 2007; Porat et al., 2008; Sivan et al., 2011).

The Nile-sediment fluxes responsible for the Kurkar ridges have continued to operate throughout the Holocene and are still dominant today (Ronen et al., 2005; Zviely et al., 2006). Currently, the rates of sand supplied by wind- and wave-induced longshore currents gradually decrease northwards and end in the Haifa Bay depositional sink (Fig. 1a; Inman and Jenkins, 1984; Zviely et al., 2006). The initiation and timing of current wind-induced coastal sand build-up is based on luminescence and radiocarbon ages of in situ land snails and relative age estimations from archaeological relicts. Dates sampled offshore (Porat et al., 2003b; Goodman-Tchernov et al., 2009) and in Israel's central coastal plain suggest that the coastal sand unit accumulated since ~6 ka (Fig. 1; Engelmann et al., 2001; Frechen et al., 2001; Kadosh et al., 2004; Roskin et al., 2015). The connection between coastal landscape, sedimentological characteristics and human occupation has been determined for the Caesarea-Atlit (Fig. 1) coast, during the Pre-Pottery Neolithic B period (that ends at ~8 ka) and the Chalcolithic period (ending ~5.1 ka) when humans settled on the dried dark silty clay, while later in the Middle Bronze age IIA period, (~4 ka), they settled on the aeolianite ridges (Galili and Nir, 1993; Galili et al., 1997; Sivan et al., 2004a, 2011).

The area offshore of Hadera was found suitable for conducting a case study aimed at verifying the influence of sea-level changes on an open coastal sedimentary sequence. Moreover the area is suitable for investigating the relationship between topography, and hydrology with the coastline evolution on the basis of: (1) its particular location between two streams (Taninim and Alexander; Fig. 1b), (2) the inclusion of various morphologies (Kurkar ridges, coastal dunes, marshlands and stream), which provide the optimal conditions for studying their interplay with sea level-changes through time.

3. Methods

3.1. Compilation of existing datasets

Existing shallow bathymetry, sub-bottom profiling and borehole data (both geotechnical and lithological) were collected from governmental offices, academic institutes and commercial companies. The bathymetric and sub-bottom profiling measurements were undertaken by the Israeli Oceanographic and Limnological Research (IOLR) in 2007 on board of the *RV Adva*, which was equipped by the following devices: a single-beam Odom Echotrack Df-3200 MK2 echo-sounder operating at 209 kHz frequency; and a Datasonic CAP-6600 chirp sub-bottom profiler operating in the frequency range of 2 to 7 kHz with a shot interval of 0.25 s and a vertical resolution of 0.15 m. A Trimble differential GPS provided navigation at horizontal precisions <1 m (Golan, 2007). The measurements were generally conducted in the E to W direction and consisted of 13 lines perpendicular to the coast, spaced 50 m apart and two shore normal lines extending from elevations of −2 to −28 m (Fig. 2), relative to the Israel Land Survey Datum (mILSD).

One hundred terrestrial and offshore boreholes were also made available for the purposes of this study. These were acquired in different surveys since the 1970s ranging in depths from 5 to 50 m below the drilling surface. Out of the 100 boreholes, 40 were drilled offshore on behalf of the Israel Electric Corporation between 1978 and 1980 (see Fig. 2 for location).
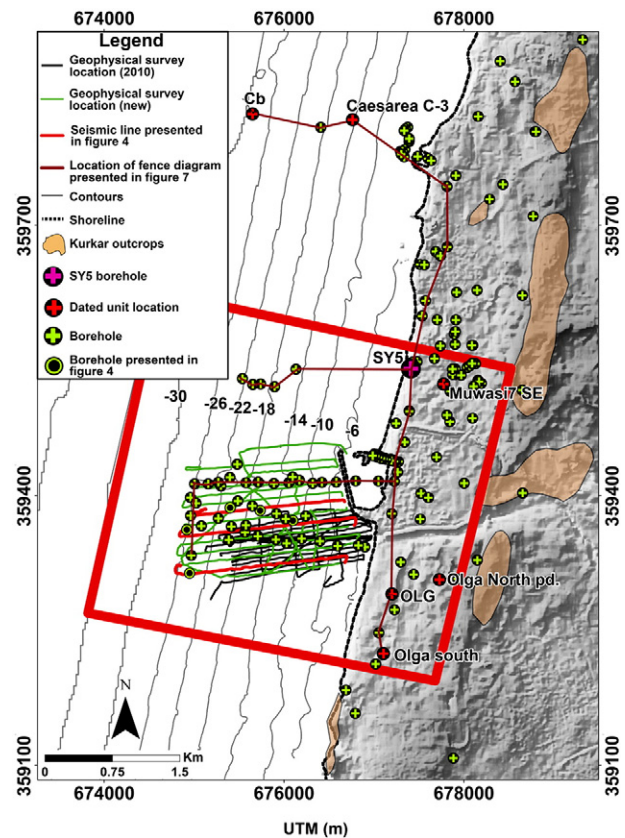

Fig. 2. Enlargement of the study area showing the location of the boreholes and seismic data. The black circles with a red cross are the locations of dated units from previous studies which include: Cb (Neev et al., 1978), Caesarea C-3 (Goodman-Tchernov et al., 2009), Muwasi 7Se, Olga North bp. Olga south (Roskin et al., 2015), OLG (Frechen et al., 2001). The black circle with the purple cross is the location of borehole SY5; for analysis see Fig. 8.

3.2. Newly acquired datasets

In order to fill the gaps in the extent of the existing datasets, new geophysical and sedimentological datasets were obtained. The survey was conducted on board *RV Adva* using the equipment and acquisition parameters from the 2010 survey. Over 110 km of seismic profiles were acquired in an area encompassing ~34 km². The survey grid consisted of 15 lines perpendicular to the coastline, spaced 100 m apart extending from −4 to −27 mILSD. Spatial referencing were added and interpretation of the seismic profiles were performed in Paradigm and Petrel software packages. Constant velocities of 1500 m/s and 1750 m/s were considered for seawater and unconsolidated sediment, respectively. These are based on published results of a refraction survey, which was conducted in the Hadera's shallow shelf (Almagor and Nir, 1977; Nir, 1979). Both the existing and newly acquired datasets were integrated into a single geospatial database using ArcGIS.

The seismic survey was complemented by core SY5, which retrieved 9.6 m of sediments using a Geo-probe 6620DT vibrocorer device 1 km north of Hadera harbor onshore at an elevation of 1.2 mILSD (Fig. 2 for location). The borehole location and elevation were measured using a Proflex 500 DGPS with precisions of 1 and 5 cm respectively. The constant datum used through the study enabled to efficiently connect the various datasets and seamlessly link between the shallow shelf and coastal zone. Following drilling operations, core SY5 was transported to the University of Haifa for storage at 4 °C. Following this step, the core was sectioned lengthwise for visual lithological description and further sedimentological measurements. Samples for granulometry and Total Carbon (IC/TOC) were retrieved from the main lithological units. The samples were to later be measured using a Malvern laser diffraction particle-size analyzer and a Primacs^SLC TOC Analyzer at the Basin Analysis and Petrophysical Laboratory (PetroLab), the University of Haifa.

4. Results

4.1. Seismic stratigraphy

The seismic stratigraphic analysis of the shallow continental shelf offshore Hadera reveals seven seismic units:

4.1.1. Acoustic basement (AB)

The acoustic basement (Fig. 3a) is characterized by a seismically transparent unit with no internal reflectors, topped by an irregular, uneven and rugged set of reflections (S1; Fig 4), which extends over the entire study area from elevations of −4 m to −28 mILSD and dips westwards at ~1.4° (Figs. 3a, 4). A ~N-S striking elongate structural high is recognized at elevations of −24 to −26 mILSD and at a distance of ~1.4 km parallel to the current coastline (Fig. 5). This morphological feature has a maximum width of 200 m, with crests that are sitting higher than 8 m above the surrounding surface topography. The main axis of this structure is perpendicularly dissected by five ~3 m deep troughs at water depths of −24 to −26 mILSD.

4.1.2. Unit F1

Unit F1 is characterized by an acoustically transparent to semi-transparent seismic facies, occasionally intercalated by low amplitude, high frequency chaotic discontinuous reflections (Fig. 3b). The unit thickness varies between 0 and 6 m (Fig. 4), and its top is bounded by three high to medium amplitude reflections, marking three irregular surfaces (S2, S3 and S4; Fig. 4). The combined surface of F1 (S2, S3 and S4; Fig. 5) dips westward at an angle of ~1° with an identifiable 400 m wide topographical high which covers the S1's ridge-resembling feature (Figs. 4, 5). The crest is situated 1.4 km west and parallel to the present shoreline (Fig. 5) and has a morphology that dips 2.5° westward. The morphological high divides the surface into two main sloping (<0.5°) depressions that are located 1 km and 2.1 km from the shoreline with
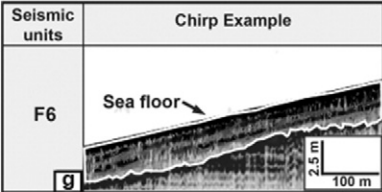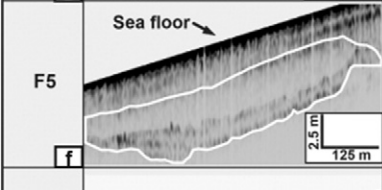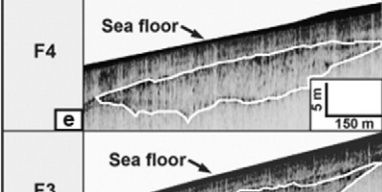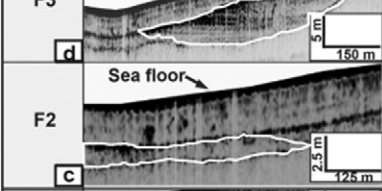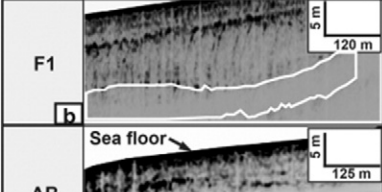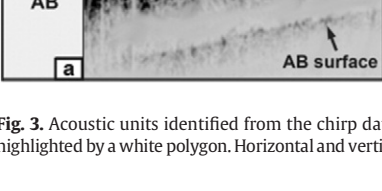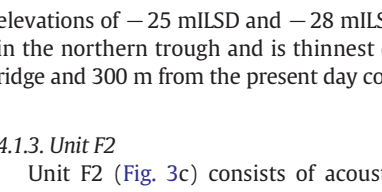

Seismic units	Chirp Example	Description
F6	Sea floor. VE = ~20. 2.5 m / 100 m	Consisting of continuous sub-parallel west dipping reflections. VE = ~20.
F5	Sea floor. 2.5 m / 125 m	This thin lens-shaped facies consisting of several continuous horizontally gently west dipping reflections. VE = ~25.
F4	Sea floor. 5 m / 150 m	Lens-shaped progradaded facies consting of chaotic high amplitude and low frequency reflections. VE = ~15.
F3	Sea floor. 5 m / 150 m	Lens-shaped progradaded facies which consist of high amplitude continuous reflections. The reflectors are sub-horizontal and sub-parallel E-W clinoforms. VE = ~15.
F2	Sea floor. 2.5 m / 125 m	The unit is acoustically semi-transparent and discontinuous low-amplitude with high frequency chaotic reflections. VE = ~12.
F1	5 m / 120 m	Acoustically transparent - semi-transparent unit. Occasionally intercalated by low amplitude chaotic reflections. VE = ~12.
AB	Sea floor. 5 m / 125 m. AB surface	The top of the unit is irregular and diffractive, constituting the acoustic basement. VE = ~12.

Fig. 3. Acoustic units identified from the chirp data acquired in Hadera. The facies are highlighted by a white polygon. Horizontal and vertical scales are shown for each example.

elevations of −25 mILSD and −28 mILSD, respectively. F1 is thickest in the northern trough and is thinnest directly above the surface S1 ridge and 300 m from the present day coastline (Fig. 6).

4.1.3. Unit F2

Unit F2 (Fig. 3c) consists of acoustically semi-transparent and discontinuous low-to-medium amplitude, and occasional high frequency and chaotic, reflections. This seismic unit is bounded between S2 and S5 below and above, respectively, and its thickness varies by up to 3 m. F2 is truncated in the eastern, up slope direction by units F3 (Fig. 4b, c) and F4 while the elevation of its top ranges from −30 to −32 mILSD in the westernmost edge of the survey area.

4.1.4. Unit F3

Unit F3 (Fig. 3d) is found in the northern parts of the survey (Fig. 6), and consists of high amplitude, continuous sub-horizontal reflectors and sub-parallel, west-trending clinoforms (Fig. 4a–d). F3 represent a lens-shape prograded infill package, toplapping the S5 and downlapping surface S3 (Fig. 4). The base of F3 (S3) is truncated landwards by the base of unit F5 (S4). The thickness of the facies varies between 0 and 5 m, being thicker in the southern parts of the S3 depression at elevations of −29 mILSD while it is thinnest above the S1 morphological high at elevations of −17 mILSD and 1250 m from the present day coastline (Fig. 6).
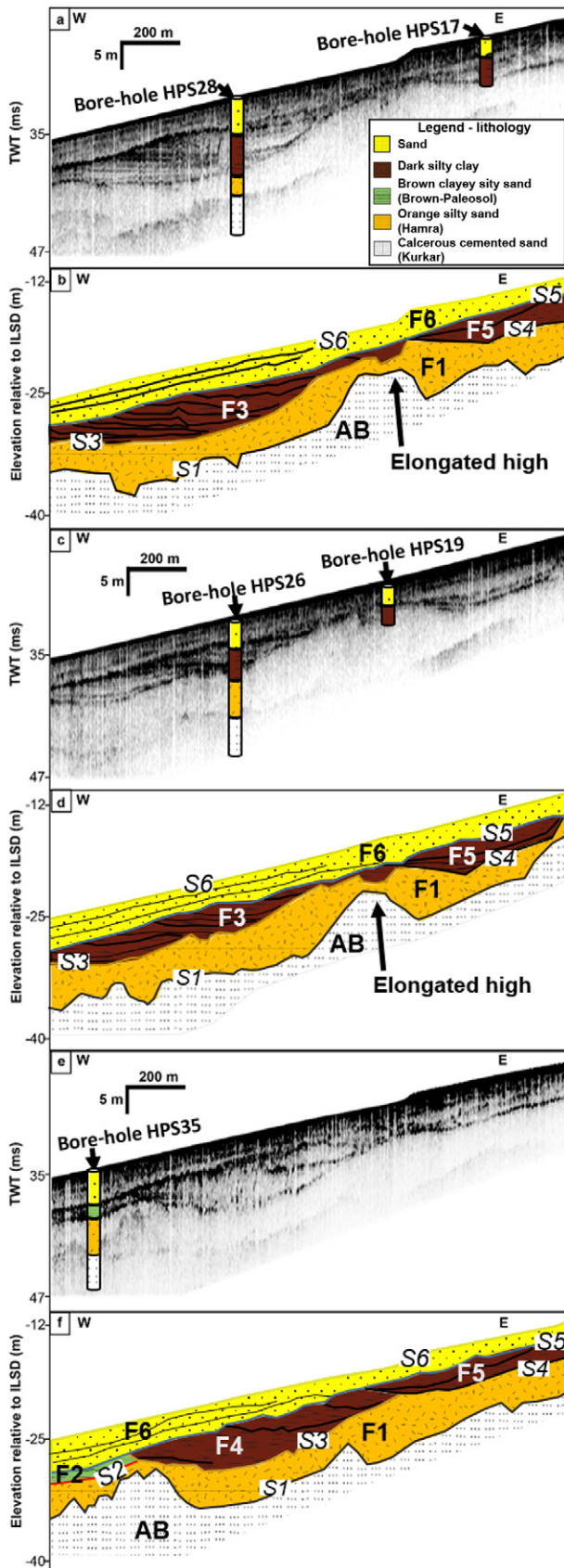
Fig. 4. Hadera's shallow coastal shore-normal seismic sections (a, c and e) and their interpretation (b, d and f) which was done on the basis of boreholes HPS19, HPS26, HPS35, HPS17 and HPS28. The location of the seismic section and boreholes is displayed in Fig. 2.

4.1.5. Unit F4

Unit F4 (Fig. 3e) is found only in the southern parts of the survey, and consists of mostly chaotic high amplitude and low frequency reflections (Fig. 4e, 4f). Overall it appears to represent a lens-shape prograded infill package, toplapping the S5 and downlapping surface S3 (Fig. 4). The base of F4 (S3) is truncated landwards by the base of Unit F5 (S4). The thickness of the unit varies between 4 and 7 m, being thicker in the southern parts of the S3 depression with elevations of −30 mILSD and thinnest above the S3 morphological high at elevations of −17 mILSD and 1300 m from the present day coastline (Fig. 6).

4.1.6. Unit F5

Unit F5 (Fig. 3f) consists of several continuous sub-horizontal sub-parallel reflections which onlap S4 seawards and toplap S5 landward (Fig. 4). These reflections are shoreward bounded by weak to moderate discontinuities and chaotic reflectivity. F5 appears to represent a thin lens-shaped prograded sedimentary fill, which is confined at the bottom by S4. F5 is generally dipping ~0.8° seaward, its thickness varies between 0.5 and 4 m, thickest above S1 eastern depression and thinnest above S1 ridge and in its southern and northern boundaries (Figs. 5, 6).

4.1.7. Unit F6

Unit F6 (Fig. 3g) is characterized by continuous, medium amplitude, medium frequency, sub-horizontal and sub-parallel reflectors. The reflections onlap the unit's lower boundary S5 shoreward; S5 truncates previously deposited sediments of units 4 and 5 (Fig. 4). S5 extends up to 2.1 km from the present shoreline, with elevation ranging between −5 mILSD adjacent to the shoreline to −26 mILSD in its westernmost stretch (Fig. 5). The surface has a general westward dip of 0.8°. F6 thickness varies between 1 and 5 m, is thickest in its northern boundary and at water depths larger than 17 m (Fig. 6).

Facies F6 is confined at the top by surface S6 which corresponds to the present-day sea floor. The S6 surface (Fig. 5) is generally dipping 0.9° west and its elevation ranges from 0 to −28 mILSD in the westernmost edge of the survey areas. A west-trending linear depression, up to 250 m wide and 3 m deep, is evident at elevations of −7 to −25 mILSD offshore Hadera's power plant harbor (Figs. 5, 6).

4.2. Lithostratigraphy

Up to five litho-stratigraphic units (Kurkar, Hamra, Brown-Paleosol, dark silty clay and sand) are identified in both the N-S and E-W sections, inferred from the available borehole data (location of fence diagram is presented in Fig. 2), which range from 12 to −14 mILSD and from 12 to −40 mILSD, respectively (Fig. 7). The surface of the Kurkar is evident in most of the boreholes and reveals an uneven surface with topographic highs and lows both onshore and offshore Hadera.

Stratigraphic analysis reveals that the thickest unconsolidated sedimentary units occupy the depressions in between the Kurkar ridges, while they are thinnest on top of the Kurkar highs (Fig. 7). The Hamra facies, which is identified in most of the boreholes, covers the Kurkar and has a thickness that ranges from 1 to 8 m. In the boreholes the topography of the Hamra surface mirrors that of the Kurkar throughout the study zone. The Hamra is, in turn, covered by a 1 to 3 m-thick Brown-Paleosol unit in the western parts of the area, between −22 and −26 mILSD and in a few zones in the vicinity of the shoreline. In the western parts of the study area, from a depth of −28 to −20 mILSD, the dark silty clay facies is seen deposited on top of the Hamra and/or Brown-Paleosol, varying in thickness between 2 and 6 m. Onshore the unit is scarce and is only seen in one section. A sandy facies covers the identified units onshore and offshore at times also including shell fragments or finer (silt) fractions. The sand unit is evident from elevations of −26 to 11 mILSD, with thicknesses varying between 1 and 7 m.
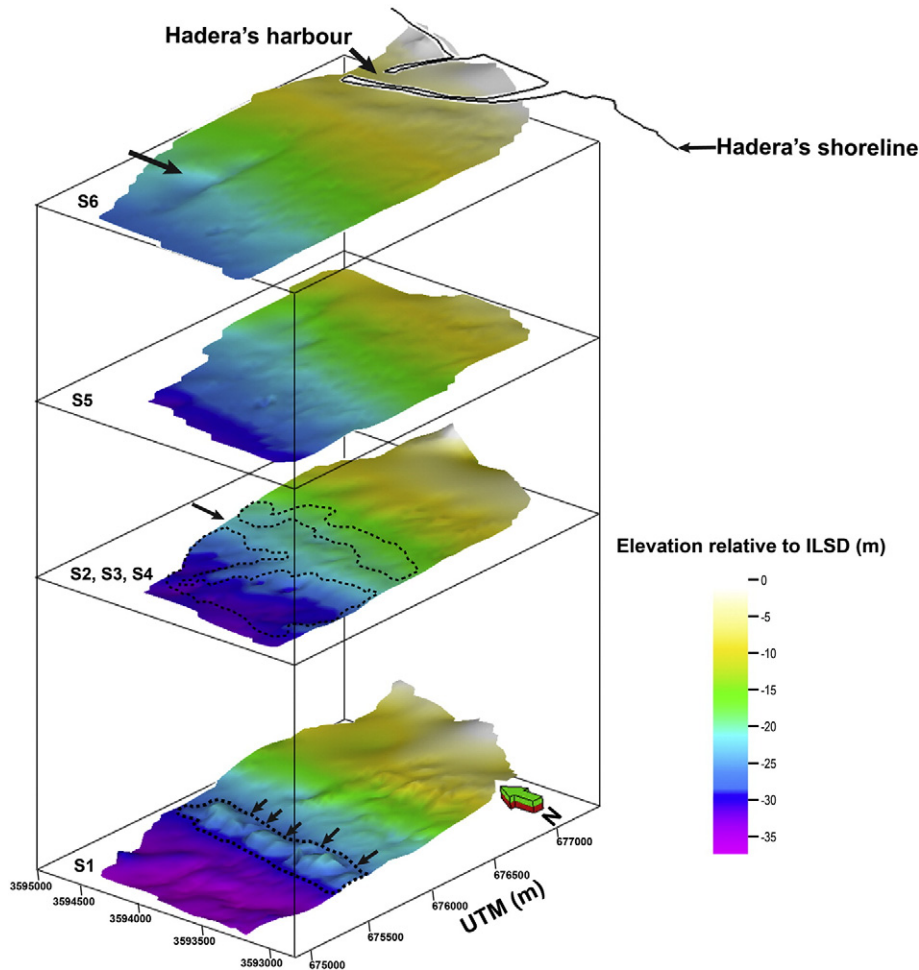
Fig. 5. Elevation map of the seismic unit surfaces and counterpart features. The elongated-high and five cutting troughs of surface S1 are annotated by a dashed polygon and arrows respectively. The topographical high of the combined surface S2, S3 and S4 is marked by an arrow while the two bordering depressions are annotated by dashed polygons. The west trending linear morphological depression of surface S6 is highlighted by an arrow.

All five litho-stratigraphic units are present in core SY5 (Fig. 8). The sedimentological description and corresponding properties are described for each unit:

- The lowermost unit the Kurkar, starting at −8.2 mILSD and reaching the borehole's bottom, is composed of fine bright yellow (Fig. 8a) sand mixed with small size Kurkar clasts (Fig. 8f). Inorganic carbon values decrease upward and rang between 2 and 4% (Fig. 8g). These characteristics and the elevation of the Kurkar unit in nearby onshore and offshore boreholes (Fig. 7) led to the identification of this unit.
- Overlying the Kurkar is a Hamra unit which is composed of an orange fine silty sand (Fig. 8a, b, e, f). The unit is 1.2 m thick (−8.2 to −7 mILSD) and is homogenous with high fractions of sand (Fig. 8f). These characteristics and the elevation of the Hamra unit in nearby boreholes located onshore and offshore (Fig. 7) was used for its identification.
- Covering the Hamra is a Brown-Paleosol unit which consists of a dark brown clayey silty sand. The unit is 3.2 m thick (−7 to −3.8 mILSD: Fig. 8b, c, e), mostly homogenous and has relatively higher fractions of silt and clay (Fig. 8f). However, between −5.3 to −4.8 m depth (ILSD), thin yellowish sand layers are evident (Fig. 8a, f). Root remains are detected between −5.3 to −4.6 m (ILSD). These characteristics and the elevation of the paleosol unit in nearby boreholes located onshore and offshore (Fig. 7) led to the unit's identification.
- Overlying the paleosol is a 0.5 m thick (−3.8 to −3.3 mILSD) grey-dark grey clayey silty sand with a few yellow 1–3 cm sand patches. Sediment composition of clay and silt fractions is lower than 35%

(Fig. 8f) while fractions of organic carbon range between 0.2 and 0.8% (Fig. 8g). The identification of this unit was based on these characteristics along with the elevation of a similar characterized unit located in onshore and in offshore boreholes (Fig. 7).
- Covering the dark silty clay is a 4.3 m thick greyish yellow sand unit with scattered bivalve fragments spotted between 0.8 and −0.3 mILSD. Inorganic carbon values decrease downward ranging between 1 and 3.5% (Fig. 8g). From depths of −1.8 (ILSD) m the unit becomes less homogenous consisting of finer grain fractions and sand aggregates (Fig. 8a, f, d). From −2.5 mILSD, the unit's dampness increases, and it gradually becomes water saturated. This unit is also evident in various neighboring boreholes both onshore and offshore.

4.3. Sedimentological and stratigraphical interpretation

The seismic units were correlated with the stratigraphy and lithology based on the geometrical relations between the different units, their respective seismic facies, the morphological features identified on coastal outcrops, litho-stratigraphical relations and the sedimentological correspondence with the boreholes. The lithological description of the acoustic basement surface and the six seismic units are presented from bottom to top, as follows:

The morphology of the acoustic basement S1 surface resembles the elevation differences, dipping angles, irregularity and shore parallel direction of the Kurkar, as observed on the adjacent coast (Gvirtzman et al., 1998; Sivan et al., 2004a; Frechen et al., 2001: Fig. 2). These
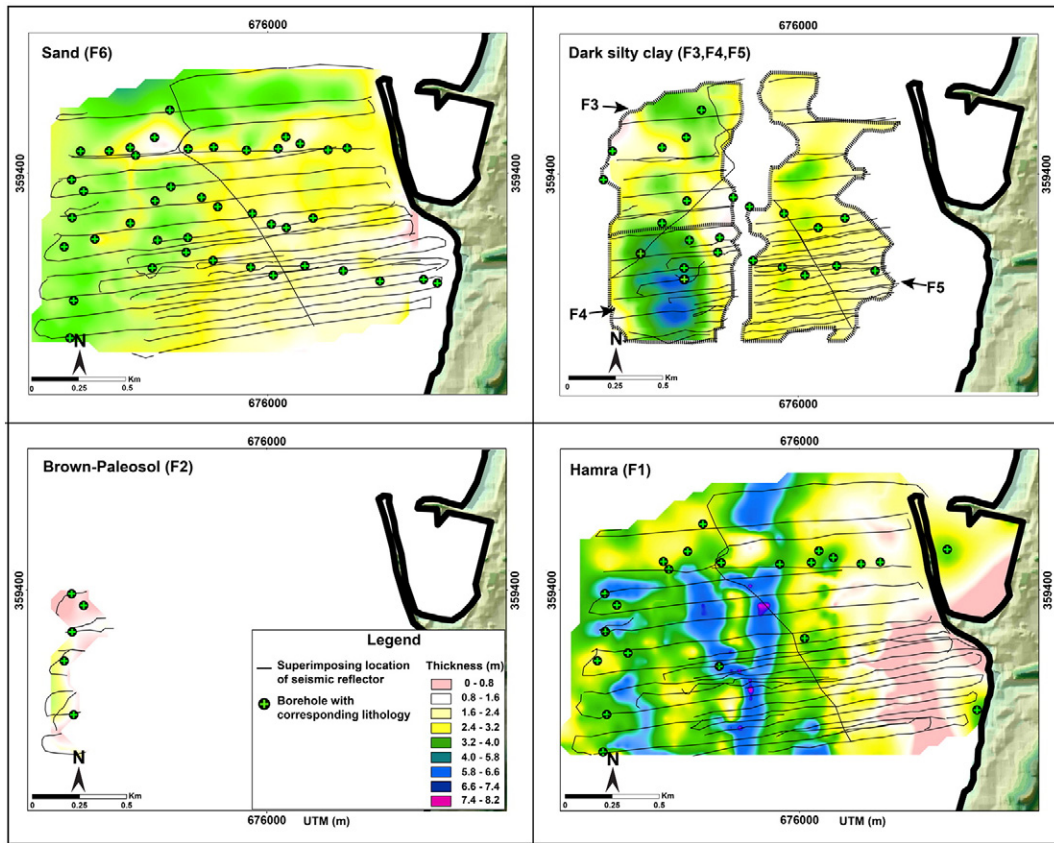
Fig. 6. Isopach map of Hadera's seismic litho-stratigraphies. Each surface is presented with its corresponding seismic reflector and matching borehole-lithology. The litho-facies are presented from young (top left) to old (bottom right).

morphological characteristics also match those of Kurkar as interpreted from a uniboomer seismic section by Neev et al. (1978) in water depths of 5 to 35 m offshore Caesarea (~2.5 km north of Hadera; Fig. 1). Moreover, this surface is identified and directly correlated to the seismic sections in 22 offshore boreholes. Taken together, this evidence

leads to the identification of the acoustic basement as the top of the Kurkar surface.

Over the entire study area, the Kurkar is directly overlain by seismic unit F1. This seismic unit is penetrated by 12 boreholes all of which show Hamra sediments at this depth (Fig. 6). Covering the Hamra,
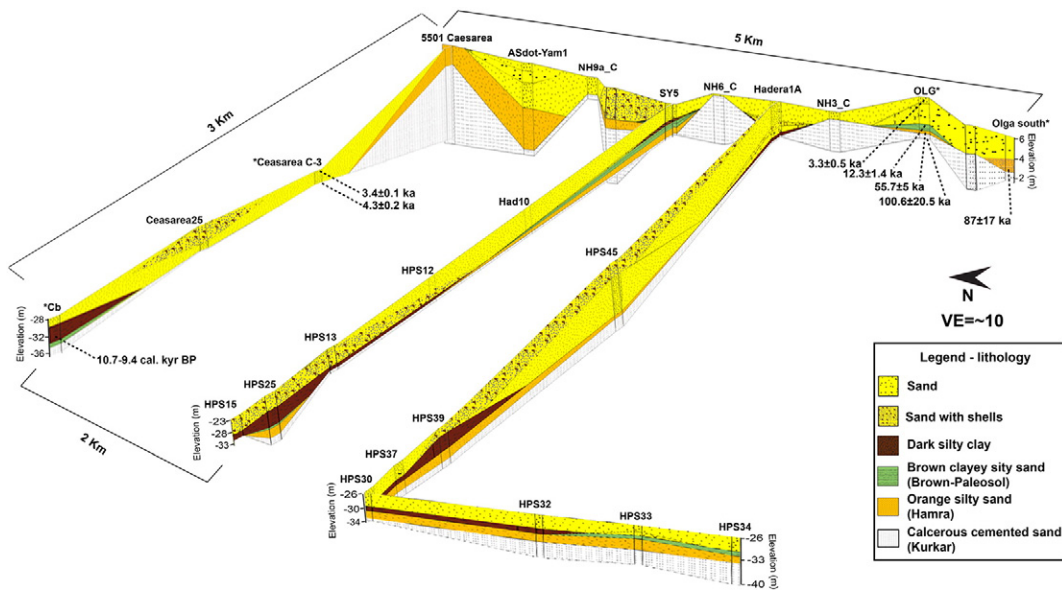

Fig. 7. Fence diagram presenting the litho-stratigraphies of Hadera coastal and shallow shelf area according to borehole lithology and core SY5. Boreholes in which the lithologies have been dates in previous studies are marked with *. These include: Cb (Neev et al., 1978), Caesarea C-3 (Goodman-Tchernov et al., 2009), Olga south (Roskin et al., 2015), OLG (Frechen et al., 2001). The location of the boreholes is displayed in Fig. 2.
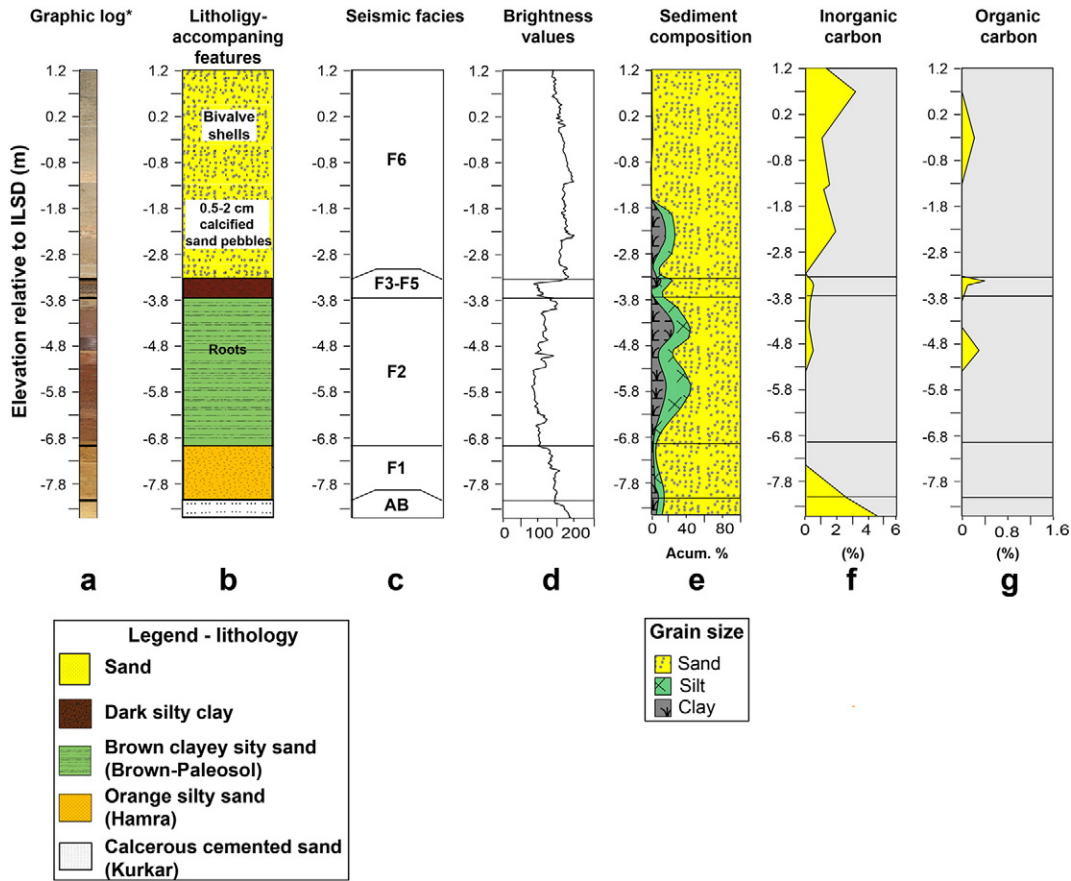
Fig. 8. Borehole SY5 (location is displayed in Fig. 2) with lithology description, accompanying features, analogous seismic facies, graphic analysis (a–d), sedimentological and geochemical results (e–g).

from water depths of −26 to −28 mILSD, is a 2 m thick lens-shape unit (Fig. 6) which is directly sampled by 5 boreholes, and can be correlated to the bordering coastal area sequences (Fig. 6). Thus seismic unit F2 correlates to the Brown-Paleosol unit.

Three lens-shaped fill units (F3, F4 and F5) cover the Hamra and truncate the Brown-paleosol unit in the western boundary of the study area. These seismic units F3, F4 and F5 are all identified as dark silty clay units based on depth correspondences of these three units' surfaces in 23 boreholes. Units F3 and F4 display similar morphologies, thicknesses and lithology throughout the correlated boreholes. However, marked differences of reflectivity geometries are observed between unit F3 in the north and unit F4 in the south (Fig. 3). While the southern sections (F4; Fig. 6) consist of chaotic low-amplitude reflections (Fig. 4e), the northern ones (F3; Fig. 6) consist of subparallel sub-horizontal high amplitude reflections (Fig. 4a). These dissimilarities suggest different depositional mechanisms for the similar silty clay sediments. Finally, the topmost unit (F6), when correlated with 40 boreholes is identified as a sandy unit with minor shells and silty sands components (Fig. 6).

5. Discussion

5.1. Chronological framework

The correlation between the litho-stratigraphical units and previously dated sequences (Figs. 2, 7) also allows a chronology to be assigned to the described units. The deepest and oldest detectable surface identified across the entire study area is the top of the Kurkar sequence.

The Kurkar surface, on the terrestrial side and in the shallow offshore, has been dated between ~101 and ~50 ka (Gvirtzman et al.,

1998; Frechen et al., 2001; Porat et al., 2003a; Sivan and Porat, 2004; Zviely et al., 2006). These ages represent the depositional age of the sand, which occurred before and during the lithification process (Yaalon, 1967; Gavish and Friedman, 1969; Sivan and Porat, 2004). Based on these dates, and the Kurkar ages obtained in Hadera's coastal area (for location see Fig. 7; Frechen et al., 2001; Roskin et al., 2015) we hypothesize a similar chronology for the submerged Kurkar surface (Table 1).

A Hamra unit overlies the Kurkar and, in the western parts, is overlain by a Brown-Paleosol sequence (Fig. 4). The correlation of these units to the onshore Hamra and Brown-Paleosol (Figs. 7, 8) suggests that the units were deposited between ~87 to ~55 ka for the Hamra and between ~50 to ~11 ka for the Brown-Paleosol (Table 1). As discussed by Sivan and Porat (2004), the wide age ranges for these units suggest that the Hamra and Paleosol were deposited laterally over time with no direct association to sea levels. Although no direct dating has been carried out offshore, the extent and boundaries of the Hamra and Brown-Paleosol can be clearly delineated in the seismic surveys and corresponding boreholes (Figs. 4, 6).

Overlying the Hamra unit and truncating the western Brown-Paleosol boundary are two dark silty clay units, which are interpreted as representing wetland units (F3/F4 and F5; Figs. 4, 5, 6). The western and eastern lens-shaped seismic units are characterized as different wetland facies based on their seismic facies appearances, thickness, elevations differences and depositional environments which are divided by a topographic high. These facies stratigraphically corresponds to the coastal-wetland silty clays located in the Carmel coast (Fig. 1b) described by Kadosh et al. (2004); Sivan et al. (2004a); Cohen-Seffer et al. (2005), and Sivan et al. (2011). The base of the western wetland unit (F3/F4) is correlated to a wetland facies sampled in core Cb, 2.5 km north of the study area (Fig. 7),

Table 1

Dated litho-facies in the Israel's north-central coastal and its adjacent shallow marine area (see Figs. 1b and 2 for location). The unit elevation values are compared to Israel Land Survey Datum ILSD.

Borehole and reference	Unit/lithology of sample	Depth of unit compared to ILSD		Age range (ka)	
		Top	Bottom	Top	Bottom
Muwasi BB (5)	Sand	1		3.3 ± 0.1[a]	
Caesarea c-3 (2)	Sand	−15.8	−16.1	3.4 ± 0.1[a]	4.3 ± 0.2[a]
Muwasi 7SE (5)	Sand	3.4	2.5	0.86 ± 0.1[a]	4.8 ± 0.7[a]
OLG (1)	Sand	16.8	15	3.3 ± 0.5[a]	5.3 ± 0.7[a]
MAM-B (5)	Dark silty clay	−8	−9.3	8.7–9.0 cal	9.2–9.5 cal
Cb-Ceasarea (3)	Dark silty clay	−32		9.4– 10.7 cal	
MAM-B (4)	Brown clayey silty sand (Brown-Paleosol)	−10.4	−11.4	11.1–11.2 cal	23.6–24 cal
OLG (1)	Brown clayey silty sand (Brown-Paleosol)	8.8	4.8	12.3 ± 1.4[b]	50.5 ± 9[b]
OLG (1)	Orange silty sand (Hamra)	7.1	2.1	55.7 ± 5[b]	
Olga South (5)	Orange silty sand (Hamra)	2.6	1.6		87 ± 17[a]
OLG (1)	Calcareous cemented sand (Kurkar)	5.5	4.3	54.7 ± 9.1[b]	100.6 ± 20.5 [b]
MAM-B (4)	Calcareous cemented sand (Kurkar)	−12		59.6 ± 5.2[a]	
Olga North pd. (5)	Calcareous cemented sand (Kurkar)	0.4		92 ± 18[a]	
MAM-A (4)	Calcareous cemented sand (Kurkar)	−12		101 ± 11[a]	

cal − [14]C calibrated dates.
Referenced Chrono-stratigraphy data: (1) Frechen et al. (2001); (2) Goodman-Tchernov et al. (2009); (3) Neev et al. (1978); (4) Cohen-Seffer et al. (2005); (5) Roskin et al. (2015).
[a] OSL dates.
[b] IRSL dates.

which was dated to 10.7–9.4 cal. Kyr BP. This correlation is proposed due to the corresponding sub-bottom topography, stratigraphy, equivalent distance from the present-day shoreline (~2 km) and elevation (base elevation of −32 m ILSD) discussed by Neev et al. (1978). The inner seismic reflections of the wetland deposits are cut at the unit's top (Fig. 4) indicating that the surface of the western (F3/F4) and eastern (F5) units mark an erosional unconformity. Taking into account the sea-level curve of the Mediterranean from the LGM to present times (Fig. 9; Sivan et al., 2004b), and the elevations of the ravinement surfaces which extend from −28 to −12 mILSD, it is proposed that the wetland units eroded between ~9 ka and ~8 ka (Table 1). Nilotic sand (F6) was transported landward and deposited on top of the dark silty clay units (F3/F4 and F5; Figs. 4, 9). OSL chronologies sampled offshore Caesarea in equivalent water depths (Reinhardt et al., 2006; Goodman-Tchernov et al., 2009) and also onshore Hadera (Frechen et al., 2001; Roskin et al., 2015) indicate that sand stabilization started ~6 ka. The ages leave a time gap of ~2000 years between the wetland drying phase and

the beginning sand deposition. It is most probable that the sand started to accumulate in these areas during the transgression (now ranging between -28 m to -15 m) ~8 ka. However, since the area was subjected to high energy, which characterizes the surf zone, the sand was bleached due to sunlight exposer causing the age values to be younger.

5.2. Paleogeographical reconstruction of the ancient drainage system

The top of the Kurkar and Hamra surfaces shows clear indications of a lowstand drainage system (Fig. 10). The channel locations were computed using the ArcGIS Hydrology toolset. The calculation modeled the hydrological flow for the interpolated submerged unit surfaces. The procedure was done in four steps: (1) identification and sink filling; (2) flow direction calculation; (3) calculating the flow accumulation; and (4) creation of the stream network. Location in which the paths could be the result of interpolation artifacts are marked by a dashed line.
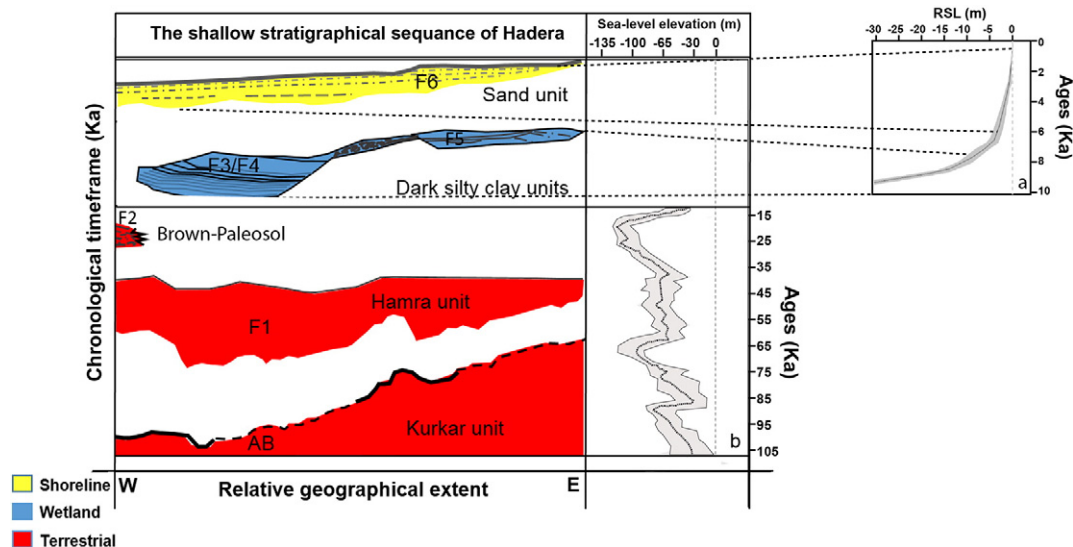

Fig. 9. Wheeler diagram of Hadera shallow coastal shelf stratigraphical sequence. The stratigraphical units are displayed according to their depositional environment, depositional epoch, location and sea-level fluctuations. The deposition period and sea-level changes are presented in relative time. Please note that there is a time overlap for the Kurkar (AB) Hamra (F1) and paleosol units (F2) and a hiatus between the wetland episode (~11 to ~8 ka) and the beginning sand deposition (~6 ka). The interglacial is demonstrated for the early Holocene (a) (after Sivan et al., 2001) and the last 105,000 years (b) (after Rohling et al., 2014). The envelope for both pots (shading) demonstrates the upper and lower limits.
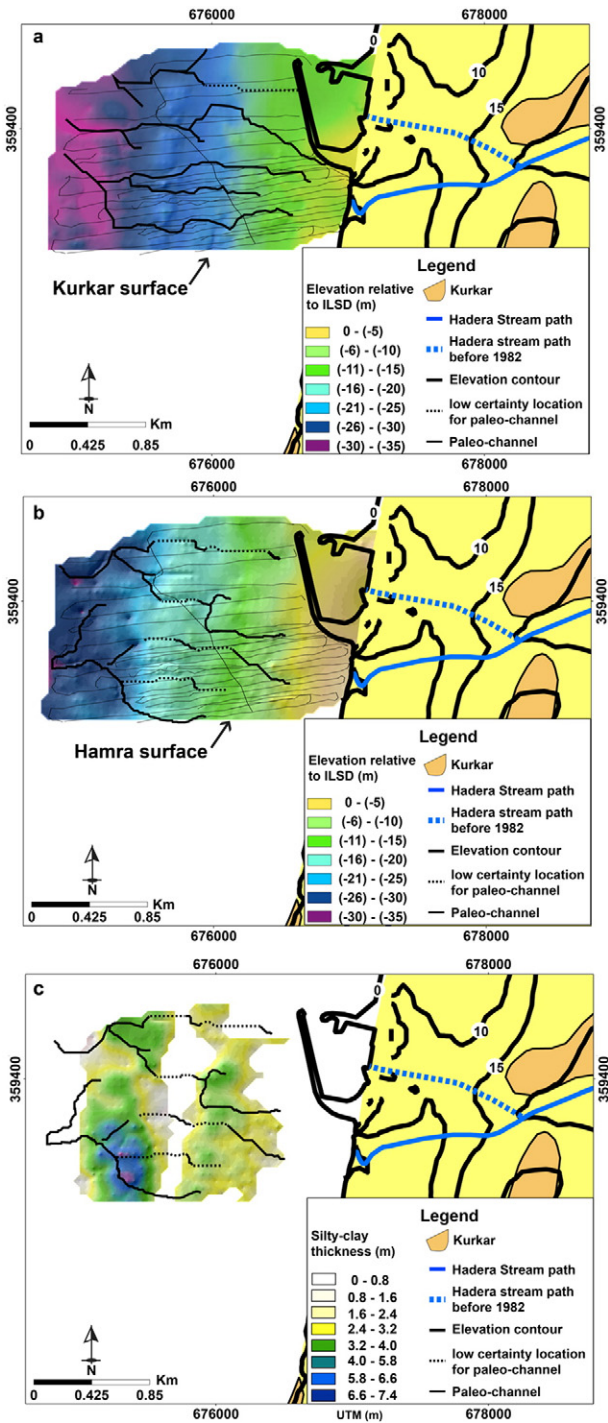
Fig. 10. Late Pleistocene to Early Holocene paleo-drainage system of Hadera (grey line). The drainage system was computed for the Kurkar (AB surface; a) and Hamra (F1 surface; b); and is presented against the dark silty clay isopach layer (F3–F5; c).

The Kurkar and Hamra paleo-drainage systems correlates in direction and channel width (3 to 5 m) to the adjacent Hadera stream (Fig. 10). The Hadera stream is one of the most substantial coastal rivers in Israel (Lichter et al., 2011). The stream extends more than 50 km long with a drainage basin that covers an area of approximately 600 km². As a result of the construction of Hadera's power plant in the 1980's the stream's natural path was altered and its route was moved south, a few hundred m from its natural route (Fig. 10). The Kurkar and Hamra drainage system begins about 300 m from the present-day coastline and unlike the current coastal system possibly consisted of 6

and 5 paths respectively both trending in E-W directions. Then, 1.5 km from the modern shoreline, the three southern creeks of the Kurkar unite to one route, while the Hamra's two northern and three southern creeks unite, forming two main routes.

Further, the greatest accumulations of the overlying dark silty clay sediments are found in the deepest topographic lows of this incised Hamra surface and near the paleo-drainage intersections (Fig. 10c). This spatial correlation would suggest that the Hadera stream played a major role in contributing depositing material into these wetlands during the early Holocene. We also hypothesize that the reflection geometries of the fill units (F3/F4) differ between the northern and southern (Figs. 3, 4) areas because of the differences in the proximity to the drainage system channels (Fig. 10). The unstructured facies located in the southern parts is interpreted to be related to higher fluvial energy and continuous supply of homogenous fine material. The western located acoustically well layered geometry results from lower energy draping of these sediments in this wetland environment. Thus, Hadera's paleo-stream affected the sedimentary depositional patterns of the western and eastern wetlands.

5.3. Paleoenvironmental evolution

As a result of lower sea levels throughout most of the study's timeframe (between ~100 and ~9 ka), Hadera's offshore area was exposed and the shoreline was located between ~3 and ~13 km to the west of its present location (Almagor et al., 2000; Waelbroeck et al., 2002; Lambeck and Purcell, 2005; Hughes et al., 2013). In the final stages of the transgression (between ~9 and ~3 ka) the study area was flooded by the rising sea (Sivan et al., 2001, 2004a; Porat et al., 2008). The sea-level transgression shaped the deposition, preservation and erosion patterns of unconsolidated sediments and altered the currently submerged morphological features at Hadera.

The Kurkar surface was lithified between ~101 and ~50 ka in a terrestrial environment on the exposed shelf (Fig. 9). After its cementation the irregular surface was subjected to atmospheric and fluvial (Hadera paleo-stream path; Fig. 10) erosion which made it rugged and channelized (Friedman, 1964; Yaalon, 1967; Gavish and Friedman, 1969; Schattner et al., 2010).

Following the Kurkar's formation, Nilotic-based aeolian sediments infilled the Kurkar depressions and eventually covered its peaks (Figs. 4, 7) (Gvirtzman and Wieder, 2001; Sivan and Porat, 2004; Cohen-Seffer et al., 2005). The sand was later pedogenized in an oxidizing environment, in which the Hamra evolved (Gvirtzman et al., 1998; Sivan and Porat, 2004) reaching thicknesses of up to ~8 m. The boundary between the Hamra and the Brown-Paleosol is acoustically distinguished (Figs. 3a, 4). The distinctive soil-sequence boundaries are hypothesized to be linked to alteration in deposition of finer material as seen in Hadera's borehole based litho-stratigraphy (Fig. 7) and sedimentological analysis of SY5 (Fig. 8). The two units were pedogenized under different climatic conditions which resulted in finer material variations and differences in hue, and carbonate content (Yaalon, 1997; Gvirtzman et al., 1998; Gvirtzman and Wieder, 2001).

During the early Holocene (~10.5 to ~8 ka), sea-levels rose from ~−45 to ~−15 m (Fig. 9; Fairbanks, 1989; Bard et al., 1990, 1996; Lambeck and Bard, 2000; Sivan et al., 2001; Lambeck and Chappell, 2001; Sivan et al., 2004b; Berné et al., 2007) and the Israeli shoreline migrated ~1.5 km shoreward. Over this timeframe, four probable contributing factors led to the formation of Hadera's wetlands (Figs. 4, 6):

1. The coastal groundwater was elevated as a response to the sea-level rise and its shoreward migrating trend. The high levels of the aquifer flooded the topographic lows of the Hamra unit (Sivan et al., 2011).
2. The shelf flooding reduced the stream gradient, which consequently reduced the stream drainage energy.

3. Drainage was obstructed by growing volumes of Nilotic sediments transported shoreward as a result of the transgressing sea.
4. Wetter and warmer conditions occurred between 10.5 and 7.5 ka (Bar-Matthews et al., 2003), which consequently induced an increase in stream flow conditions that swamped the lowland areas.

At around ~8 ka, the rising sea flooded the eastern-most part of the wetlands. Nilotic sand was transported shoreward and started to accumulate on the wetland surface by ~6 ka. During this time wave and wind induced currents transported the sand to the shoreline and it was windblown inland. Then, by ~4 ka, when the shoreline reached its current location (Sivan et al., 2001) sand was windblown up to 2.5 km inland (Roskin et al., 2015) later to form Hadera's sand dune field.

6. Conclusion

This is the first high resolutions combined geophysical and geological study to be conducted along the open coast of Israel (<30 m) that combines marine and terrestrial data and which covers a time period which spans over more than 100 ka. The combination of continuous marine seismic data with core data drilled on land enables a 4D reconstruction (including the time dimension) of an area that was long exposed to changing environmental conditions, and later was flooded by the sea.

The chronostratigraphy is based on correlation to adjacent dated coastal and marine stratigraphical units. The reconstruction revealed that the stratigraphy of this area is dominated by aeolian and fluvial processes operating during sea level lowstands. Only later, during the Holocene, is the landscape directly affected by a marine transgression, and the landward approaching shorelines. The units overlying the Pleistocene Kurkar were deposited in three environments: 1) the oldest Hamra/paleosol units were deposited and pedogenized in a terrestrial environment over the course of thousands of years; 2) the early Holocene's wetland-silty clay units were deposited in a calm, fresh to brackish, water environment with increasing siltation in response to rising sea levels; and 3) the Nilotic sand unit, which was deposited in a shallow marine environment over the last 8000 years.

The coastal changes recorded from the open coastline environment at Hadera contrast with the previous studies undertaken in more sheltered embayments on the Israeli coast (i.e. Haifa Bay: Zviely et al., 2006; Porat et al., 2008). In these enclosed areas the rapid transgression during the early part of the Holocene led to rapid onshore migration of the coastline, reaching a maximum of 3 km inland of the modern-day coastline at ~4 ka. Then, once sea levels reached its current position and in response to the Nile-sediment input from the west, and local wetland and fluvial sediment input from the east, the coastline prograded until retreating back to its current position by ~2 ka. This late phase progradation is absent from the Hadera section which is characterized by continuous transgression until ~4 ka when it reached its present location.

The understanding gained from the study will serve as an analogue to other shallow marine and adjacent coastal environments that have formed under similar conditions (e.g. open sea, with sand supply source etc.). This reconstruction can also be of use for archaeological and engineering purposes. Archaeologists can use the 4D litho-stratigraphical mapping for targeting ancient habitation which changed according to the (now submerged) surface lithology, distance from paleo-water sources and rising sea levels. A connection between wetland sequences and ancient settlement having already been established in Israel's central coastal area, suggests that there is high archaeological potential offshore. Finally, engineers can make use of such high-resolution subsurface data for future infrastructure planning intended to be built/buried in or on the shelf's shallow subsurface. These include marines and harbors, gas pipes, electricity cables and communication network.

References

Allard, J., Chaumillon, E., Féniès, H., 2009. A synthesis of morphological evolutions and Holocene stratigraphy of a wave-dominated estuary. The Arcachon lagoon, SW France. Cont. Shelf Res. 29, 957–969.
Almagor, G., Nir, Y., 1977. Detailed bathymetric and shallow seismic survey off the site for the M. D. Electric Station Near HaderaIsrael Geological Survey, Report GSI/1/77, Jerusalem.
Almagor, G., Hall, J.K., 1984. Morphology of the Mediterranean continental margin of Israel. Bull. Geol. Surv. Israel 77, 31.
Almagor, G., 1993. Continental slope processes off northern Israel and southernmost Lebanon and their relation to onshore tectonics. Mar. Geol. 112, 151–169.
Almagor, G., Gill, D., Perath, I., 2000. Marine sand resources offshore Israel. Mar. Georesour. Geotechnol. 18, 1–42.
Anderson, J.B., Wallace, D.J., Simms, A.R., Rodriguez, A.B., Milliken, K.T., 2014. Variable response of coastal environments of the northwestern Gulf of Mexico to sea-level rise and climate change: implications for future change. Mar. Geol. 352, 348–366.
Anzidei, M., Antonioli, F., Benini, A., Lambeck, K., Sivan, D., Serpelloni, E., Stocchi, P., 2011. Sea-level change and vertical land movements since the last two millennia along the coasts of southwestern Turkey and Israel. Quat. Int. 232, 1–20.
Bard, E., Hamelin, B., Fairbanks, R.G., 1990. U–Th ages obtained by mass spectrometry in corals from Barbados: sea level during the past 130,000 years. Nature 346, 456–458.
Bard, E., Hamelin, B., Arnold, M., Montaggioni, L., Cabioch, G., Faure, G., Rougerie, F., 1996. Deglacial sea-level record from Tahiti corals and the timing of global meltwater discharge. Nature 382, 241–244.
Bar-Matthews, M., Ayalon, A., Gilmour, M., Matthews, A., Hawkesworth, C.J., 2003. Sea–land oxygen isotopic relationships from planktonic foraminifera and speleothems in the Eastern Mediterranean region and their implication for paleorainfall during interglacial intervals. Geochim. Cosmochim. Acta 67, 3181–3199.
Bersezio, R., Giudici, M., Mele, M., 2007. Combining sedimentological and geophysical data for high-resolution 3-D mapping of fluvial architectural elements in the Quaternary Po plain (Italy). Sediment. Geol. 202, 230–248.
Bates, M.R., Richard Bates, C., Briant, R.M., 2007. Bridging the gap: a terrestrial view of shallow marine sequences and the importance of the transition zone. J. Archaeol. Sci. 34, 1537–1551.
Belknap, D.F., Kraft, J.C., 1985. Influence of antecedent geology on stratigraphic preservation potential and evolution of Delaware's barrier systems. Mar. Geol. 63, 235–262.
Belknap, D.F., Mart, Y., 1999. Sea-level lowstand in the east Mediterranean-late Pleistocene coastal terraces offshore northern Israel. J. Coast. Res. 15, 399–412.
Berné, S., Jouet, G., Bassetti, M.A., Dennielou, B., Taviani, M., 2007. Late glacial to Preboreal sea-level rise recorded by the Rhône deltaic system (NW Mediterranean). Mar. Geol. 245, 65–88.
Cawthra, H.C., Bateman, M.D., Carr, A.S., Compton, J.S., Holmes, P.J., 2014. Understanding Late Quaternary change at the land–ocean interface: a synthesis of the evolution of the wilderness coastline, South Africa. Quat. Sci. Rev. 99, 210–223.
Cohen-Seffer, R., Greenbaum, N., Sivan, D., Jull, T., Barmeir, E., Croitoru, S., Inbar, M., 2005. Late Pleistocene–Holocene marsh episodes along the Carmel coast, Israel. Quat. Int. 140-141, 103–120.
Davis, R.A., Hayes, M.O., 1984. What is a wave dominant coast? Mar. Geol. 60, 313–329.
Davis, M., Matmon, A., Rood, D.H., Avnaim-Katav, S., 2012. Constant cosmogenic nuclide concentrations in sand supplied from the Nile River over the past 2.5 m.y. Geology 40, 359–362.
Emery, K.O., Bentor, Y.K., 1960. The continental shelf of Israel. Bull. Geol. Surv. Israel 26, 25–41.
Emery, K.O., Neev, D., 1960. Mediterranean beaches of Israel. Bull. Geol. Surv. Israel 26, 1–24.
Engelmann, A., Neber, A., Frechen, M., Boenigk, W., Ronen, A., 2001. Luminescence chronology of upper Pleistocene and Holocene aeolianites from Netanya South-Sharon coastal plain, Israel. Quat. Sci. Rev. 20, 799–804.
Fairbanks, R.G., 1989. A 17, 000-year glacio-eustatic sea level record: influence of glacial melting rates on the Younger Dryas event and deep-ocean circulation. Nature 342, 637–642.

Frechen, M., Dermann, B., Boenig, W., Ronen, A., 2001. Luminescence chronology of aeolianites from the section at Givat Olga Coastal Plain of Israel. Quat. Sci. Rev. 20, 805–809.

Frechen, M., Neber, A., Dermann, B., Tsatskin, S., Boenig, W., Ronen, A., 2002. Chronostratigraphy of aeolianites from the Sharon Coastal Plain of Israel. Quat. Int. 89, 31–44.

Frechen, M., Neber, A., Alexander, B., 2004a. Chronology of Pleistocene sedimentary cycles in the Carmel Coastal plain of Israel. Quat. Int. 121, 41–52.

Frechen, M., Neber, A., Tsatskin, A., Boenig, W., Ronen, A., 2004b. Chronology of Pleistocene sedimentary cycles in the Carmel Coastal Plain of Israel. Quat. Int. 121, 41–52.

Friedman, G.M., 1964. Early diagenesis and lithification in carbonate sediments. J. Sediment. Res. 34, 777–813.

Galili, E., Weinstein-Evron, M., 1985. Prehistory and palaeoenvironments of submerged sites along the Carmel Coast of Israel. Pale'orient 11, 37–51.

Galili, E., Nir, Y., 1993. The submerged Pre-Pottery Neolithic water well of Atlit-Yam, Northern Israel, and its paleoenvironmental implications. The Holocene 3, 265–270.

Galili, E., Stanley, D.J., Sharvit, Y., Weinstein-Evron, M., 1997. Evidence for earliest Olive-Oil Production in submerged settlements off the Carmel Coast, Israel. J. Archaeol. Sci. 24, 1141–1150.

Galili, E., Zviely, D., Ronen, A., Mienis, H.K., 2007. Beach deposits of MIS 5e high sea stand as indicators for tectonic stability of the Carmel coastal plain, Israel. Quat. Sci. Rev. 26, 2544–2557.

Gavish, E., Friedman, G.M., 1969. Progressive diagenesis in Quaternary to Late Tertiary carbonate sediments: sequence and time scale. J. Sediment. Res. 39, 980–1006.

Golan, A., 2007. Shallow geophysical survey in Hadera. IOLR Report (H2/2007. 19 pp. (In Hebrew)).

Golik, A., Rosen, S.D., 1999. Management of the Israeli coastal sand resources. Israel Oceanographic and Limnological Research, Report H 28/98 Submitted to the Mediterranean Action Plan and the Ministry of Environment, Israel (70 pp).

Goodman-Tchernov, B.N., Dey, H.W., Reinhardt, E.G., McCoy, F., Mart, Y., 2009. Tsunami waves generated by the Santorini eruption reached Eastern Mediterranean shores. Geology 37, 943–946.

Gvirtzman, G., Netser, M., Katsav, E., 1998. Last-Glacial to Holocene Kurkar ridges, hamra soils, and dune fields in the coastal belt of central Israel. Isr. J. Earth Sci. 47, 27–46.

Gvirtzman, G., Wieder, M., 2001. Climate of the last 53,000 years in the eastern Mediterranean, based on soil-sequence stratigraphy in the coastal plain of Israel. Quat. Sci. Rev. 20, 1827–1849.

Hampson, G.J., Storms, E.A., 2008. Geomorphological and sequence stratigraphic variability in wave-dominated, shoreface-shelf parasequences. Sedimentology 50, 667–701.

Hughes, P.D., Gibbard, P.L., Ehlers, J., 2013. Timing of glaciation during the last glacial cycle: evaluating the concept of a global 'Last Glacial Maximum' (LGM). Earth Sci. Rev. 125, 171–198.

Inman, D.L., Jenkins, S.A., 1984. The Nile Littoral Cell and Man's Impact on the Coastal Zone of the Southeastern Mediterranean. In: ASCE Proceedings of the 19th Conference on Coastal Engineering, Houston, TX. pp. 1600–1617.

Kadosh, D., Sivan, D., Kutiel, H., Weinstein-Evron, M., 2004. A late quaternary paleoenvironmental sequence from Dor, Carmel coastal plain, Israel. Palynology 28, 143–157.

Lambeck, K., Bard, E., 2000. Sea-level change along the French Mediterranean coast for the past 30,000 years. Earth Planet. Sci. Lett. 175, 203–222.

Lambeck, K., Chappell, J., 2001. Sea level change through the last glacial cycle. Science 292, 679–686.

Lambeck, K., Purcell, A., 2005. Sea-level change in the Mediterranean Sea since the LGM: model predictions for tectonically stable areas. Quat. Sci. Rev. 24, 1969–1988.

Lichter, M., Klein, M., Zviely, D., 2011. Dynamic morphology of small south-eastern Mediterranean river mouths: a conceptual model. Earth Surf. Process. Landf. 36, 547–562.

Mart, Y., Belknap, D.F., 1991. Origin of Late Pleistocene submerged marine terraces on the outer continental shelf. Geo-Mar. Lett. 11, 66–70.

Mauz, B., Hijma, M.P., Amorosi, A., Porat, N., Galili, E., Bloemendal, J., 2013. Aeolian beach ridges and their significance for climate and sea level: concept and insight from the Levant coast (East Mediterranean). Earth Sci. Rev. 121, 31–54.

Mendoza, U., Ayres Neto, A.C., Abuchacra, R., Fernandes Barbosa, C.G., Figueiredo, A.C., Gomes, M., Belem, A.L., Capilla, R., Albuquerque, A.L., 2014. Geoacoustic character, sedimentology and chronology of a cross-shelf Holocene sediment deposit off Cabo Frio, Brazil (southwest Atlantic Ocean). Geo-Mar. Lett. 34, 297–314.

Michelson, H., 1970. The Geology of the Carmel Coast (MSc thesis) the Hebrew University, Jerusalem 61 pp. (In Hebrew).

Neev, D., Almagor, G., Arad, A., Ginzburg, A., Hall, J.K., 1976. The geology of the southern Mediterranean Sea. Bull. Geol. Surv. Israel 68, 1–47.

Neev, D., Shachnai, E., Hall, J.K., Bakler, N., Ben Avraham, Z., 1978. The young (post Lower Pliocene) geological history of the Caesarea Structure. Isr. J. Earth Sci. 27, 43–64.

Nir, Y., 1979. Detailed bathymetric and shallow seismic survey off the site for the M. D. Electric Station near Hadera. Israel Geological Survey, Report GSI/1/79, Jerusalem.

Peterson, C.D., Vanderburgh, S., Roberts, M.C., Jol, H.M., Phipps, J., Twichell, D.C., 2010. Composition, age, and depositional rates of shoreface deposits under barriers and beach plains of the Columbia River littoral cell, USA. Mar. Geol. 273, 62–82.

Pomerancblum, M., 1966. The distribution of heavy minerals and their hydraulic equivalents in sediments of the Mediterranean continental shelf of Israel. J. Sediment. Res. 36, 162–179.

Porat, N., Avital, A., Frechen, M., Almogi-Labin, A., 2003a. Chronology of upper Quaternary offshore successions from the southeastern Mediterranean Sea, Israel. Quat. Sci. Rev. 22, 1191–1199.

Porat, N., Wintle, A.G., Ritte, M., 2003b. Mode and timing of Kurkar and Hamra formation, central coastal plain, Israel. Isr. J. Earth Sci. 53, 13–25.

Porat, N., Sivan, D., Zively, D., 2008. Late Holocene embayment and sedimentological infill processes in Haifa Bay, SE Mediterranean. Isr. J. Earth Sci. 57, 21–31.

Reinhardt, E.G., Goodman, B.N., Boyce, J.I., Lopez, G., van Hengstum, P., Rink, W.J., Mart, Y., Raban, A., 2006. The tsunami of 13 December AD 115 and the destruction of Herod the Great's harbor at Caesarea Maritima, Israel. Geology 34, 1061–1064.

Rohling, E.J., Foster, G.L., Grant, K.M., Marino, G., Roberts, A.P., Tamisiea, M.E., Williams, F., 2014. Sea-level and deep-sea-temperature variability over the past 5.3 million years. Nature 508, 477–482.

Ronen, A., Golik, A., Neber, A., Tsatskin, A., Boenig, W., Beiles, A., 2005. Pleistocene and Holocene pattern of sand migration along the Mediterranean littoral of Israel. Isr. J. Earth Sci. 54, 187–198.

Roskin, J., Sivan, D., Shtienberg, G., Roskin, E., Porat, N., Bookman, R., 2015. Natural and human controls of the Holocene evolution of the beach, aeolian sand and dunes of Caesarea (Israel). Aeolian Res. 19, 65–85.

Schattner, U., Lazar, M., Tibor, G., Ben-Avraham, Z., Makovsky, Y., 2010. Filling up the shelf — a sedimentary response to the last post-glacial sea rise. Mar. Geol. 278, 165–176.

Sivan, D., Gvirtzman, G., Sass, E., 1999. Quaternary stratigraphy and paleogeography of the Galilee coastal plain, Israel. Quat. Res. 51, 280–294.

Sivan, D., Wdowinski, S., Lamback, K., Galili, E., Raban, A., 2001. Holocene sea-level changes along the Mediterranean coast of Israel, based on archaeological observations and numerical model. Palaeogeogr. Palaeoclimatol. Palaeoecol. 167, 101–117.

Sivan, D., Eliyahu, D., Raban, A., 2004a. Late Pleistocene to Holocene wetlands now covered by sand, along the Carmel Coast, Israel, and their relation to human settlement: an example from Dor. J. Coast. Res. 20, 1035–1048.

Sivan, D., Lambeck, K., Toueg, R., Raban, A., Porath, Y., Shirman, B., 2004b. Ancient coastal wells of Caesarea Maritima, Israel, an indicator for relative sea level changes during the last 2000 years. Earth Planet. Sci. Lett. 222, 315–330.

Sivan, D., Porat, N., 2004. Late Pleistocene contemporaneous formation of calcareous aeolianite (Kurkar) and paleosol (Hamra) in the Carmel coast, Israel. Palaeogeogr. Palaeoclimatol. Palaeoecol. 211, 95–106.

Sivan, D., Greenbaum, N., Cohen-Seffer, R., Sisma-Ventura, G., Almogi-Labin, A., 2011. The origin and disappearance of the late Pleistocene–early Holocene short-lived coastal wetlands along the Carmel coast, Israel. Quat. Res. 76, 83–92.

Sneh, A. Y., Bartov, Rosensaft, M., 1998. Geological Map of Israel, 1:200,000, 4 Sheets. Israel Geological Survey.

Stanley, D.J., Warne, A.G., 1998. Nile Delta in its destruction phase. J. Coast. Res. 14, 795–825.

Stoker, M.S., Bradwell, T., Howe, J.A., Wilkinson, I.P., McIntyre, K., 2009. Late glacial ice-cap dynamics in NW Scotland: evidence from the fjords of the Summer Isles region. Quat. Sci. Rev. 28, 3161–3184.

Toker, E., Sivan, D., Stern, E., Shirman, B., Tsimplis, M., Spada, G., 2012. Evidence for centennial scale sea-level variability during the Medieval Climate Optimum (Crusader Period) in Israel, eastern Mediterranean. Earth Planet. Sci. Lett. 315-316, 51–61.

Twichell, D.C., Cross, V.A., Peterson, C.D., 2010. Partitioning of sediment on the shelf offshore of the Columbia River littoral cell. Mar. Geol. 273, 11–31.

Vanderburgh, S., Roberts, M., Peterson, C., Phipps, J., Herb, A., 2010. Transgressive and regressive deposits forming the barriers and beachplains of the Columbia River Littoral Cell, USA. Mar. Geol. 273, 32–43.

Waelbroeck, C., Labeyrie, L., Michel, E., Duplessy, J.C., McManus, J., Lambeck, K., Balbon, E., Labracherie, M., 2002. Sea-level and deep water temperature changes derived from benthic foraminifera isotopic records. Quat. Sci. Rev. 21, 295–305.

Wieder, M., Gvirtzman, G., Netzer, M., 1997. Origin of clayey soils on aeolian dust in the central coastal plain of Israel. In: Shoba, S., Gerasimova, M., Miedema, R. (Eds.), Soil Micromorphology: Diversity, Diagnostics, Dynamics. IWMSM, Moscow - Wageningen, pp. 196–203.

Yaalon, D.H., 1967. Factors affecting the lithification of eolianite and interpretation of its environmental significance in the coastal plain of Israel. J. Sediment. Res. 37, 1189–1199.

Yaalon, D.H., 1997. Soils in the Mediterranean region: what makes them different? Catena 28, 157–169.

Yoo, D.G., Kim, S.P., Chang, T.S., Kong, G.S., Kang, N.K., Kwon, Y.K., Nam, S.L., Park, S.C., 2014. Late Quaternary inner shelf deposits in response to late Pleistocene–Holocene sea level changes: Nakdong River, SE Korea. Quat. Int. 344, 156–169.

Zecchin, M., Baradello, L., Brancolini, G., Donda, F., Rizzetto, F., Tosi, L., 2008. Sequence stratigraphy based on high-resolution seismic profiles in the late Pleistocene and Holocene deposits of the Venice area. Mar. Geol. 253, 185–198.

Zecchin, M., Brancolini, G., Tosi, L., Rizzetto, F., Caffau, M., Baradello, L., 2009. Anatomy of the Holocene succession of the southern Venice lagoon revealed by very high-resolution seismic data. Cont. Shelf Res. 29, 1343–1359.

Zviely, D., Sivan, D., Ecker, A., Bakler, N., Rohrlich, V., Galili, E., Boaretto, E., Klein, M., Kit, E., 2006. Holocene evolution of the Haifa Bay area, Israel, and its influence on ancient tell settlements. The Holocene 16, 849–861.

Zviely, D., Kit, E., Klein, M., 2007. Longshore sand transport estimates along the Mediterranean coast of Israel in the Holocene. Mar. Geol. 238, 61–73.